



HAL
open science

Stability of a Crank-Nicolson Pressure Correction Scheme Based on Staggered Discretizations

Franck Boyer, Fanny Dardalhon, Céline Lapuerta, Jean-Claude Latché

► **To cite this version:**

Franck Boyer, Fanny Dardalhon, Céline Lapuerta, Jean-Claude Latché. Stability of a Crank-Nicolson Pressure Correction Scheme Based on Staggered Discretizations. 2012. hal-00721597v1

HAL Id: hal-00721597

<https://hal.science/hal-00721597v1>

Preprint submitted on 28 Jul 2012 (v1), last revised 3 May 2013 (v2)

HAL is a multi-disciplinary open access archive for the deposit and dissemination of scientific research documents, whether they are published or not. The documents may come from teaching and research institutions in France or abroad, or from public or private research centers.

L'archive ouverte pluridisciplinaire **HAL**, est destinée au dépôt et à la diffusion de documents scientifiques de niveau recherche, publiés ou non, émanant des établissements d'enseignement et de recherche français ou étrangers, des laboratoires publics ou privés.

Stability of a Crank-Nicolson Pressure Correction Scheme Based on Staggered Discretizations

F. Boyer², F. Dardalhon^{1,2}, C. Lapuerta¹, J.-C. Latché¹

¹ *Institut de Radioprotection et de Sûreté Nucléaire (IRSN)
BP3 - 13115 Saint Paul-lez-Durance CEDEX, France.*

² *Aix-Marseille Université, Laboratoire d'Analyse, Topologie et Probabilités,
Centre de Mathématiques et Informatique
39 rue Joliot-Curie
13453 Marseille Cedex 13, France.*

[fanny.dardalhon, celine.lapuerta, jean-claude.latche]@irsn.fr, fboyer@latp.univ-mrs.fr

SUMMARY

In the context of Large Eddy Simulation of turbulent flows, the control of kinetic energy seems to be an essential requirement for the numerical scheme. Designing such an algorithm, *i.e.* as less dissipative as possible while being simple, for the resolution of variable density Navier-Stokes equations is the aim of the present work. The developed numerical scheme, based on a pressure correction technique, uses a Crank-Nicolson time discretization and a staggered space discretization relying on the Rannacher-Turek finite element. For the inertia term in the momentum balance equation, we propose a finite volume discretization, for which we derive a discrete analogue of the continuous kinetic energy local conservation identity. Contrary to what was obtained for the backward Euler discretization, the dissipation defect term associated to the Crank-Nicolson scheme is second order in time. This behaviour is evidenced by numerical simulations. Copyright © 2000 John Wiley & Sons, Ltd.

KEY WORDS: Pressure correction scheme, compressible Navier-Stokes equations, stable convection operator, low-order finite element approximation

1. Introduction

We consider the time-dependent variable density Navier-Stokes equations, posed on a finite time interval $(0, T)$ and in an open, connected, bounded domain Ω in \mathbb{R}^d ($d = 2$, or 3), which is supposed to be polygonal ($d = 2$) or polyhedral ($d = 3$):

$$\begin{cases} \partial_t \rho + \operatorname{div}(\rho \mathbf{u}) = 0, \\ \partial_t(\rho \mathbf{u}) + \operatorname{div}(\mathbf{u} \otimes \rho \mathbf{u}) - \operatorname{div}(\tau(\mathbf{u})) + \nabla p = 0, \end{cases} \quad (1)$$

*Correspondence to: fboyer@latp.univ-mrs.fr

where \mathbf{u} , p and ρ are respectively the velocity, the pressure and the density of the flow. The quantity

$$\tau(\mathbf{u}) = \mu \left[\nabla \mathbf{u} + \nabla^T \mathbf{u} - \frac{2}{3} (\operatorname{div} \mathbf{u}) \mathbf{I} \right],$$

is the shear stress tensor, with μ the positive kinematic viscosity, and $\mathbf{u} \otimes \rho \mathbf{u}$ is the $\mathbb{R}^d \times \mathbb{R}^d$ -tensor of components $(\mathbf{u} \otimes \rho \mathbf{u})_{i,j} = \rho \mathbf{u}_i \mathbf{u}_j$, $\forall i, j \in \{1, \dots, d\}$. As such, System (1) is not closed. The simplest assumption yielding a self-contained problem is just supposing that ρ is a given function of space and time; the mass balance equation (*i.e.* the first relation of (1)) thus has to be considered as a constraint on the velocity, as for incompressible flows (and, indeed, choosing a constant value for ρ yields $\operatorname{div} \mathbf{u} = 0$). This equation basically plays the same role in the so-called asymptotic model for low Mach number flows [21], where ρ is given as a function of an additional unknown θ (usually, the temperature or a concentration), which satisfies a balance equation:

$$\partial_t(\rho \theta) + \operatorname{div}(\rho \theta \mathbf{u}) - \operatorname{div}(\lambda \nabla \theta) = 0, \quad \rho = \varrho(\theta). \quad (2)$$

The function $\theta \mapsto \varrho(\theta)$ is the given equation of state for the flow under study, and λ is a nonnegative diffusion coefficient.

System (1)-(2) must be supplemented by suitable boundary conditions, for instance Dirichlet conditions for \mathbf{u} and θ , or slip and Neumann conditions:

$$\mathbf{u} \cdot \mathbf{n} = 0, \quad ((\tau(\mathbf{u}) - p \mathbf{I}) \mathbf{n}) \cdot \mathbf{t} = 0, \quad \text{and} \quad \nabla \theta \cdot \mathbf{n} = 0 \quad \text{on} \quad (0, T) \times \partial \Omega, \quad (3)$$

where \mathbf{n} and \mathbf{t} are respectively the outward unit normal and tangential vectors to $\partial \Omega$. Initial conditions are given for \mathbf{u} and θ , namely $\mathbf{u} = \mathbf{u}^0$ and $\theta = \theta^0$ in Ω . We suppose that the equation of state is such that $\varrho(\theta) > 0$ if $\theta > 0$, that $\theta^0 > 0$, and that boundary conditions are such that θ remains positive at all times.

The density ρ and the velocity \mathbf{u} are known to satisfy the so-called kinetic energy identity. This relation stems from the following formal computation.

Property 1.1 (Property K.E.) *Let us assume that*

$$\partial_t \rho + \operatorname{div}(\rho \boldsymbol{\beta}) = 0,$$

for a regular field $\boldsymbol{\beta}$ and that the functions ρ and \mathbf{u} are smooth. Then, we have:

$$(\partial_t(\rho \mathbf{u}) + \operatorname{div}(\mathbf{u} \otimes \rho \boldsymbol{\beta})) \cdot \mathbf{u} = \partial_t \left(\frac{1}{2} \rho |\mathbf{u}|^2 \right) + \operatorname{div} \left(\frac{1}{2} |\mathbf{u}|^2 \rho \boldsymbol{\beta} \right). \quad (4)$$

Integrating this relation over Ω yields, assuming that $\boldsymbol{\beta} \cdot \mathbf{n} = 0$ on $\partial \Omega$:

$$\int_{\Omega} \left(\partial_t(\rho \mathbf{u}) + \operatorname{div}(\mathbf{u} \otimes \rho \boldsymbol{\beta}) \right) \cdot \mathbf{u} \, d\mathbf{x} = \frac{1}{2} \frac{d}{dt} \int_{\Omega} \rho |\mathbf{u}|^2 \, d\mathbf{x}. \quad (5)$$

Applying identity (4), with $\boldsymbol{\beta} = \mathbf{u}$, to the inner product of the momentum balance equation (second relation of (1)) with \mathbf{u} yields the so-called (local) kinetic energy identity:

$$\frac{1}{2} \partial_t(\rho |\mathbf{u}|^2) + \frac{1}{2} \operatorname{div}(\rho |\mathbf{u}|^2 \mathbf{u}) + \mathbf{u} \cdot \nabla p - \operatorname{div}(\tau(\mathbf{u})) \cdot \mathbf{u} = 0. \quad (6)$$

The first two terms of this relation are the time derivative and the transport term of the kinetic energy, respectively; the third one corresponds to the power of the pressure forces, and the last

term of the left-hand side stands for the viscous dissipation. Integrating over Ω , integrating by parts the viscous term and using the boundary conditions, we obtain the (global) kinetic energy conservation relation:

$$\frac{1}{2} \frac{d}{dt} \int_{\Omega} \rho |\mathbf{u}|^2 d\mathbf{x} + \int_{\Omega} \mathbf{u} \cdot \nabla p d\mathbf{x} + \int_{\Omega} \tau(\mathbf{u}) : \nabla \mathbf{u} d\mathbf{x} = 0. \quad (7)$$

This relation does not yield, in its present form, a stability estimate, because of the presence of the pressure term. For incompressible flows, a simple integration by parts shows that it vanishes; it may be recast as the time derivative of an energy term for barotropic compressible flows. For the low Mach number model, how to treat this term is unclear.

Obtaining a scheme satisfying a discrete analogue of (6)-(7) has many advantages.

- First, combined with additional arguments to control the pressure term, (7) yields a stability estimate, which is classically observed to considerably enhance the robustness of the scheme, especially for the computation of convection dominant flows.
- Second, in the context of Large Eddy Simulation (LES), a subgrid-scale model is introduced to simulate the (kinetic energy) dissipative role of the small structures in the momentum balance equation. It is thus crucial that the scheme respects this "physical" dissipation, *i.e.* not overwhelms the viscous dissipation term in (the discrete counterpart of) (6) by too large numerical residual terms [23, 2]. Defining these latter as the "dissipation defect", when designing a numerical scheme for LES, the aim should be to minimize the "dissipation defect".

The Marker And Cell (MAC) space discretization, first introduced in [15] and now widely used for the simulation of incompressible flow, applies to cartesian meshes and is of staggered type, with the pressure unknowns located at the cell center and the velocity normal components unknowns at the face centers. For divergence-free constant density flows, it has been observed since the middle of the sixties that the natural discrete convection operator associated to this discretization conserves the discrete kinetic energy [20], *i.e.* satisfies a discrete analogue of the integral identity (5) (of course, supposing, in this latter, a constant density ρ). Higher order convection operators, still enjoying the same property, and also a discrete analogue to the local kinetic energy transport equation (5), have been proposed in [25, 34, 35, 32]; combined with a suitable discretization of the pressure gradient term and a suitable time-marching algorithm, these results yield (discrete analogues to) the local and global kinetic energy balances (6) and (7).

Still for the MAC scheme, works for the compressible low Mach number case are more recent and scarcer. First, [26] generalized the finite difference formula of [25], to obtain a scheme which appears, from numerical experiments, to satisfy a discrete version of the global identity (7) up to a second order residual. A similar approach, adapted to cope with cylindrical coordinates, is proposed in [7]. Recently, a (structured) MAC scheme is presented in [24], followed by a discussion about its conservation properties: both global and local kinetic energy conservation are shown, in the semi-discrete setting as in the fully discrete one. However, the resulting scheme seems to be rather expensive, and more efficient alternatives with nonzero but still high order residuals are also proposed.

For related works in the colocated framework, see [8, 10, 14, 12].

In this article, we pursue the development of kinetic energy conserving schemes for low Mach number flows, with the aim to deal with unstructured staggered discretizations. Precisely speaking, we build a discrete convection operator satisfying the control of the kinetic energy and the reduction of the dissipation defect with high-order numerical residuals (discrete analogues of (4) and (5)). The approach we adopt is based on a finite volume structure for the convection operator first introduced in [1]; the approximation of the convected velocity at the face is centered, and the time-algorithm is obtained by a Crank-Nicolson technique. Then we implement this discretization in a pressure correction scheme, and make the expression of the dissipation defect explicit. This quantity appears to be formally second order in time, and is unsigned (unlike the first-order analogue term which would arise from a backward Euler discretization). It is plotted in numerical experiments, to assess the performance of the scheme.

The outline of the article is as follows. After introducing the meshes and the discrete spaces in Section 2, we deal in Section 3 with the construction of the convection operator (Subsection 3.1) and prove its stability (Proposition 1.1). The pressure correction scheme for Low Mach number flows is presented in Section 4, first in the semi-discrete setting, then in the fully discrete one (Subsections 4.1 and 4.2 respectively). The kinetic energy identity satisfied by the fully discrete scheme is established (Subsection 4.3), then the size of the dissipation defect is evaluated (Subsection 4.4). Numerical tests are presented in Section 5, they confirm theoretical results and illustrate the ability of the scheme to perform turbulent structures for large time steps.

2. Meshes and discrete spaces

Let \mathcal{M} be a decomposition of the domain Ω into quadrangles ($d = 2$) or hexahedra ($d = 3$), supposed to be regular in the usual sense of the finite element literature [5, conditions \mathcal{T}_h1 to \mathcal{T}_h5 p. 61 and 71]. We denote by \mathcal{E} the set of all faces σ of the mesh; by \mathcal{E}_{ext} the set of faces included in the boundary of Ω , by \mathcal{E}_{int} the set of internal faces (*i.e.* $\mathcal{E} \setminus \mathcal{E}_{\text{ext}}$) and by $\mathcal{E}(K)$ the faces of a particular cell $K \in \mathcal{M}$. The internal face separating the neighbouring cells K and L is denoted by $\sigma = K|L$. Moreover, we also use the notation $\sigma = K|\text{ext}$ if the face σ is in the control volume K and σ belongs to \mathcal{E}_{ext} . For each cell $K \in \mathcal{M}$ and each face $\sigma \in \mathcal{E}(K)$, $\mathbf{n}_{K,\sigma}$ stands for the unit normal vector to σ outward K . By $|K|$ and $|\sigma|$ we respectively denote the measures of the control volume K and the face σ .

The velocity \mathbf{u} and the pressure p are discretized using the so-called Rannacher-Turek element (also called rotated bilinear finite element [29]). The reference element \hat{K} is the unit d -cube (with faces colinear to the coordinate axes); the discrete functional space on \hat{K} is $\widetilde{\mathbb{Q}}_1(\hat{K})$, where $\widetilde{\mathbb{Q}}_1(\hat{K})$ is defined as follows:

$$\widetilde{\mathbb{Q}}_1(\hat{K}) = \text{span} \{1, (x_i)_{i=1,\dots,d}, (x_i^2 - x_{i+1}^2)_{i=1,\dots,d-1}\}.$$

The mapping T_K from the reference element \hat{K} to the current one K is the standard \mathbb{Q}_1 mapping. Besides, we choose the version of the element where the nodal function $\mathcal{N}_{K,\sigma}$ on the cell K is the average of the velocity through the face σ :

$$\forall K \in \mathcal{M}, \quad \forall \sigma \in \mathcal{E}(K), \quad \forall \mathbf{v} \in \mathcal{C}^\infty(K), \quad \mathcal{N}_{K,\sigma}(\mathbf{v}) = \frac{1}{|\sigma|} \int_{\sigma} \mathbf{v}|_K \, d\sigma.$$

Thus the discrete space X_h is defined as:

$$X_h = \left\{ \mathbf{v} \in (L^2(\Omega))^d; \forall K \in \mathcal{M}, \mathbf{v} \circ T_K \in \widetilde{\mathbb{Q}}_1(\hat{K})^d, \text{ and, } \forall \sigma = K|L, \mathcal{N}_{K,\sigma}(\mathbf{v}) = \mathcal{N}_{L,\sigma}(\mathbf{v}) \right\}.$$

The approximation for the velocity is thus non-conforming in $H^1(\Omega)^d$ because the space X_h is composed of discrete functions which are discontinuous through a face, and thus $X_h \not\subseteq H^1(\Omega)^d$. The set of degrees of freedom for the velocity is:

$$\{\mathbf{u}_{\sigma,i} = \mathcal{N}_{\sigma}(\mathbf{u}_i), \sigma \in \mathcal{E}, 1 \leq i \leq d\},$$

where $\mathcal{N}_{\sigma}(\mathbf{u}_i) = \mathcal{N}_{K,\sigma}(\mathbf{u}_i) = \mathcal{N}_{L,\sigma}(\mathbf{u}_i)$ if $\sigma = K|L$. We denote by $\varphi_{\sigma}^{(i)}$ the vector shape function associated to $\mathbf{u}_{\sigma,i}$, which, by definition, reads $\varphi_{\sigma}^{(i)} = \varphi_{\sigma} \mathbf{e}^{(i)}$, where φ_{σ} is the scalar shape function and $\mathbf{e}^{(i)}$ is the i^{th} vector of the canonical basis of \mathbb{R}^d , and we define \mathbf{u}_{σ} by $\mathbf{u}_{\sigma} = \sum_{i=1}^d \mathbf{u}_{\sigma,i} \mathbf{e}^{(i)}$. With these definitions, we have the identity:

$$\mathbf{u}(\mathbf{x}) = \sum_{\sigma \in \mathcal{E}} \sum_{i=1}^d \mathbf{u}_{\sigma,i} \varphi_{\sigma}^{(i)}(\mathbf{x}) = \sum_{\sigma \in \mathcal{E}} \mathbf{u}_{\sigma} \varphi_{\sigma}(\mathbf{x}), \quad \text{for a.e. } \mathbf{x} \in \Omega.$$

We respectively denote by $\nabla \mathbf{v}$ and $\text{div } \mathbf{v}$ the broken gradient and divergence of any function $\mathbf{v} \in X_h$.

The pressure belongs to the space M_h composed of piecewise constant functions:

$$M_h = \{p \in L^2(\Omega); \forall K \in \mathcal{M}, p \text{ is constant on } K\}.$$

The degrees of freedom for the pressure are consequently $\{p_K; K \in \mathcal{M}\}$. This pair of finite elements is *inf-sup* stable [3].

The unknown θ and the density are piecewise constant, and their degrees of freedom are denoted by $\{\theta_K; K \in \mathcal{M}\}$ and $\{\rho_K; K \in \mathcal{M}\}$.

For the definition of the schemes, we need a dual mesh which is defined as follows. When $K \in \mathcal{M}$ is a rectangle or a cuboid, for $\sigma \in \mathcal{E}(K)$, we define $D_{K,\sigma}$ as the cone with basis σ and with vertex the mass center of K . We thus obtain a partition of K in m sub-volumes, where m is the number of faces of the cell (*i.e.* $m = 4$ for $d = 2$ and $m = 6$ for $d = 3$), each sub-volume having the same measure $|D_{K,\sigma}| = |K|/m$. We extend this definition to general quadrangles and hexahedra, by supposing that we still have built a partition of equal-volume sub-cells, and with the same connectivities; note that this is of course always possible, but that such a volume $D_{K,\sigma}$ may be no longer a cone, since, if K is far from a parallelogram, it may not be possible to build a cone having σ as basis, the opposite vertex lying in K and a volume equal to $|K|/m$. The volume $D_{K,\sigma}$ is referred to as the half-diamond cell associated to K and σ . For $\sigma \in \mathcal{E}_{\text{int}}$, $\sigma = K|L$, we now define the diamond cell D_{σ} associated to σ by $D_{\sigma} = D_{K,\sigma} \cup D_{L,\sigma}$ (see Figure 1). For an external face $\sigma \in \mathcal{E}_{\text{ext}} \cap \mathcal{E}(K)$, D_{σ} is just the same polyhedron as $D_{K,\sigma}$. We use the following notations for the set of dual faces of the dual mesh thus built: the set of internal dual faces is referred to as $\bar{\mathcal{E}}_{\text{int}}$ and, for a particular dual cell D_{σ} , it is denoted by $\bar{\mathcal{E}}(D_{\sigma})$; the external faces of the dual mesh coincide with primal faces, and the set of dual external faces is thus denoted by \mathcal{E}_{ext} .

Second, let us turn to the construction of the fluxes $F_{\sigma,\varepsilon}$. The essential idea is to impose the following mass balance over the half dual cell:

$$F_{K,\sigma} + \sum_{\substack{\varepsilon \in \bar{\mathcal{E}}(D_\sigma) \\ \varepsilon \subset K}} F_{\sigma,\varepsilon} = -\frac{|D_{K,\sigma}|}{\delta t} (\rho_K - \rho_K^*). \quad (11)$$

For an external face σ , using $\rho_\sigma = \rho_K$, this relation is exactly (9), provided that we choose the primal mass flux $F_{K,\sigma}$ as the dual mass flux through σ (remember that σ is both a primal and dual edge), which we indeed do. For an internal face $\sigma = K|L$, combining (11) written for K and L with the definition (10) of the density and using the conservativity of the primal mass fluxes (*i.e.* $F_{K,\sigma} + F_{L,\sigma} = 0$) yields (9) once again. Let us now use the primal mass balance (8) to write (11) as:

$$F_{K,\sigma} + \sum_{\substack{\varepsilon \in \bar{\mathcal{E}}(D_\sigma) \\ \varepsilon \subset K}} F_{\sigma,\varepsilon} = \frac{|D_{K,\sigma}|}{|K|} \sum_{\sigma' \in \mathcal{E}(K)} F_{K,\sigma'} = \frac{1}{m} \sum_{\sigma' \in \mathcal{E}(K)} F_{K,\sigma'}. \quad (12)$$

Writing this relation for all the faces σ of K yields a linear system, which is singular (summing these m relations and using the conservativity of the dual mass fluxes) and has an infinity of solutions. Thanks to the form of the right-hand side of (12), selecting the one which is orthogonal to the kernel of the system, we obtain a relation of the form:

$$F_{\sigma,\varepsilon} = \sum_{\sigma' \in \mathcal{E}(K)} \alpha_{\varepsilon,\sigma'} F_{K,\sigma'},$$

where the coefficients $(\alpha_{\varepsilon,\sigma'})$ are real numbers independent of the cell K . For instance, in two dimensions, with the notations of Figure 2, we obtain for each dual mass flux $F_{\sigma,\varepsilon}$ an expression of the form:

$$F_{\sigma,\varepsilon} = \alpha_W F_W + \alpha_E F_E + \alpha_S F_S + \alpha_N F_N, \quad (13)$$

with the coefficients gathered in Table I.

Table I. Coefficients for the dual mass fluxes in Equation (13).

$F_{\sigma,\varepsilon}$	α_W	α_E	α_S	α_N
$F_{W S}$	$-3/8$	$1/8$	$3/8$	$-1/8$
$F_{S E}$	$-1/8$	$3/8$	$-3/8$	$1/8$
$F_{E N}$	$1/8$	$-3/8$	$-1/8$	$3/8$
$F_{N W}$	$3/8$	$-1/8$	$1/8$	$-3/8$

We are now in position to define a finite volume convection operator \mathcal{C}_h for any discrete fields \mathbf{u} and \mathbf{u}^* in X_h as follows:

$$\forall \sigma \in \mathcal{E}, \quad \mathcal{C}_h(\mathbf{u}, \mathbf{u}^*)_\sigma = \frac{1}{\delta t} (\rho_\sigma \mathbf{u}_\sigma - \rho_\sigma^* \mathbf{u}_\sigma^*) + \sum_{\varepsilon \in \bar{\mathcal{E}}(D_\sigma)} \frac{1}{|D_\sigma|} F_{\sigma,\varepsilon} \frac{\mathbf{u}_\varepsilon + \mathbf{u}_\varepsilon^*}{2}, \quad (14)$$

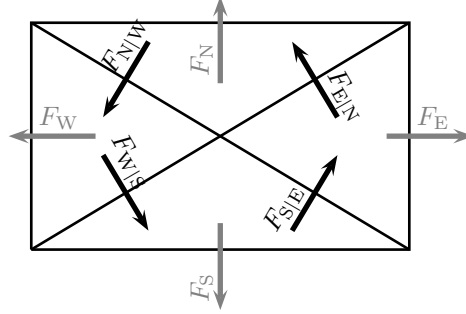


Figure 2. Notation for the mass fluxes.

with \mathbf{u}_ε ($\varepsilon \in \bar{\mathcal{E}}$) given by:

$$\mathbf{u}_\varepsilon = \begin{cases} \frac{1}{2} (\mathbf{u}_\sigma + \mathbf{u}_{\sigma'}), & \text{if } \varepsilon = D_\sigma | D_{\sigma'} \in \bar{\mathcal{E}}_{\text{int}}, \\ \mathbf{u}_\sigma, & \text{if } \varepsilon = D_\sigma | \text{ext} \in \mathcal{E}_{\text{ext}}. \end{cases} \quad (15)$$

Remark 1. With the same arguments, the construction of the convective operator and the dual mass fluxes can be generalized in three dimension. For instance, 3D computations are performed in [1].

3.2. Stability analysis of the convection operator

In this section, we prove the discrete counterpart of Property 1.1 for the convection operator given by (14)-(15).

Proposition 3.1. *Let us assume that the discrete mass balance (9) holds, for any $\sigma \in \mathcal{E}$. Provided that $F_{\sigma,\varepsilon} = 0$ for any $\varepsilon = D_\sigma | \text{ext}$, we have:*

$$\forall \sigma \in \mathcal{E}, \quad \forall \mathbf{u}, \mathbf{u}^* \in X_h,$$

$$\begin{aligned} & |D_\sigma| \mathcal{C}_h(\mathbf{u}, \mathbf{u}^*)_\sigma \cdot \left(\frac{\mathbf{u}_\sigma + \mathbf{u}_\sigma^*}{2} \right) \\ &= \frac{1}{2\delta t} |D_\sigma| \left(\rho_\sigma |\mathbf{u}_\sigma|^2 - \rho_\sigma^* |\mathbf{u}_\sigma^*|^2 \right) + \frac{1}{2} \sum_{\varepsilon = D_\sigma | D_{\sigma'}} F_{\sigma,\varepsilon} \frac{\mathbf{u}_\sigma + \mathbf{u}_\sigma^*}{2} \cdot \frac{\mathbf{u}_{\sigma'} + \mathbf{u}_{\sigma'}^*}{2} + \mathcal{R}_\sigma, \end{aligned}$$

where \mathcal{R}_σ is a remainder term given by:

$$\mathcal{R}_\sigma = -\frac{1}{8\delta t} |D_\sigma| (\rho_\sigma - \rho_\sigma^*) |\mathbf{u}_\sigma - \mathbf{u}_\sigma^*|^2.$$

We recognize at the right-hand side a discrete kinetic energy balance with a conservative finite volume discretization of the kinetic energy convection terms.

Proof. We have:

$$|D_\sigma| \mathcal{C}_h(\mathbf{u}, \mathbf{u}^*)_\sigma \cdot \left(\frac{\mathbf{u}_\sigma + \mathbf{u}_\sigma^*}{2} \right) = T_1 + T_2,$$

with

$$T_1 = \frac{1}{\delta t} |D_\sigma| (\rho_\sigma \mathbf{u}_\sigma - \rho_\sigma^* \mathbf{u}_\sigma^*) \cdot \frac{\mathbf{u}_\sigma + \mathbf{u}_\sigma^*}{2},$$

$$T_2 = \frac{\mathbf{u}_\sigma^* + \mathbf{u}_\sigma}{2} \cdot \left(\sum_{\varepsilon \in \mathcal{E}(D_\sigma)} F_{\sigma,\varepsilon} \frac{\mathbf{u}_\varepsilon + \mathbf{u}_\varepsilon^*}{2} \right).$$

The term T_1 reads:

$$T_1 = \underbrace{\frac{1}{2\delta t} |D_\sigma| (\rho_\sigma |\mathbf{u}_\sigma|^2 - \rho_\sigma^* |\mathbf{u}_\sigma^*|^2)}_{T_{1,1}} + \underbrace{\frac{1}{2\delta t} |D_\sigma| (\rho_\sigma - \rho_\sigma^*) \mathbf{u}_\sigma \cdot \mathbf{u}_\sigma^*}_{T_{1,2}}. \quad (16)$$

We now turn to T_2 . Let us introduce the following notations:

$$\bar{\mathbf{u}}_\sigma = \frac{\mathbf{u}_\sigma + \mathbf{u}_\sigma^*}{2}, \quad \forall \sigma \in \mathcal{E} \quad \text{and} \quad \bar{\mathbf{u}}_\varepsilon = \frac{\mathbf{u}_\varepsilon + \mathbf{u}_\varepsilon^*}{2}, \quad \forall \varepsilon \in \bar{\mathcal{E}}. \quad (17)$$

We get:

$$T_2 = \bar{\mathbf{u}}_\sigma \cdot \left(\sum_{\varepsilon \in \mathcal{E}(D_\sigma)} F_{\sigma,\varepsilon} \bar{\mathbf{u}}_\varepsilon \right).$$

Using $\bar{\mathbf{u}}_\sigma \cdot \bar{\mathbf{u}}_\varepsilon = |\bar{\mathbf{u}}_\sigma|^2 + \bar{\mathbf{u}}_\sigma \cdot (\bar{\mathbf{u}}_\varepsilon - \bar{\mathbf{u}}_\sigma)$, we obtain:

$$T_2 = \underbrace{|\bar{\mathbf{u}}_\sigma|^2 \sum_{\varepsilon \in \mathcal{E}(D_\sigma)} F_{\sigma,\varepsilon}}_{T_{2,1}} + \underbrace{\sum_{\varepsilon \in \mathcal{E}(D_\sigma)} F_{\sigma,\varepsilon} \bar{\mathbf{u}}_\sigma \cdot (\bar{\mathbf{u}}_\varepsilon - \bar{\mathbf{u}}_\sigma)}_{T_{2,2}}. \quad (18)$$

Let us consider the second term $T_{2,2}$. Using the identity $2\mathbf{a} \cdot (\mathbf{a} - \mathbf{b}) = |\mathbf{a}|^2 + |\mathbf{a} - \mathbf{b}|^2 - |\mathbf{b}|^2$, valid for any real vectors \mathbf{a} and \mathbf{b} , we get:

$$T_{2,2} = -\frac{1}{2} |\bar{\mathbf{u}}_\sigma|^2 \sum_{\varepsilon \in \mathcal{E}(D_\sigma)} F_{\sigma,\varepsilon} + \frac{1}{2} \sum_{\varepsilon \in \mathcal{E}(D_\sigma)} F_{\sigma,\varepsilon} (|\bar{\mathbf{u}}_\varepsilon|^2 - |\bar{\mathbf{u}}_\sigma - \bar{\mathbf{u}}_\varepsilon|^2).$$

Consequently,

$$T_2 = \frac{1}{2} |\bar{\mathbf{u}}_\sigma|^2 \sum_{\varepsilon \in \mathcal{E}(D_\sigma)} F_{\sigma,\varepsilon} + \frac{1}{2} \sum_{\varepsilon \in \mathcal{E}(D_\sigma)} F_{\sigma,\varepsilon} (|\bar{\mathbf{u}}_\varepsilon|^2 - |\bar{\mathbf{u}}_\sigma - \bar{\mathbf{u}}_\varepsilon|^2).$$

Using the discrete mass balance equation (9), we get:

$$T_2 = -\underbrace{\frac{1}{2\delta t} |D_\sigma| (\rho_\sigma - \rho_\sigma^*) |\bar{\mathbf{u}}_\sigma|^2}_{T_{2,2,1}} + \underbrace{\frac{1}{2} \sum_{\varepsilon \in \mathcal{E}(D_\sigma)} F_{\sigma,\varepsilon} (|\bar{\mathbf{u}}_\varepsilon|^2 - |\bar{\mathbf{u}}_\sigma - \bar{\mathbf{u}}_\varepsilon|^2)}_{T_{2,2,2}}.$$

First, the term $T_{2,2,1}$ may be combined with the term $T_{1,2}$ in (16), and using the definition (17) of $\bar{\mathbf{u}}_\sigma$, this gives:

$$T_{2,2,1} + T_{1,2} = -\frac{1}{8\delta t} |D_\sigma| (\rho_\sigma - \rho_\sigma^*) |\mathbf{u}_\sigma - \mathbf{u}_\sigma^*|^2 = \mathcal{R}_\sigma.$$

Second, by the centered definition (15) of the approximation of the convected velocity at the face, $T_{2,2,2}$ reads also:

$$T_{2,2,2} = \frac{1}{2} \sum_{\epsilon=D_\sigma|D_{\sigma'}} F_{\sigma,\epsilon} \bar{\mathbf{u}}_\sigma \cdot \bar{\mathbf{u}}_{\sigma'} + \frac{1}{2} \sum_{\epsilon=D_\sigma|\text{ext}} F_{\sigma,\epsilon} |\bar{\mathbf{u}}_\sigma|^2.$$

Finally, with Equation (17), we obtain:

$$T_{2,2,2} = \frac{1}{2} \sum_{\epsilon=D_\sigma|D_{\sigma'}} F_{\sigma,\epsilon} \frac{(\mathbf{u}_\sigma + \mathbf{u}_\sigma^*) \cdot (\mathbf{u}_{\sigma'} + \mathbf{u}_{\sigma'}^*)}{2} + \frac{1}{8} |\mathbf{u}_\sigma + \mathbf{u}_\sigma^*|^2 \sum_{\epsilon=D_\sigma|\text{ext}} F_{\sigma,\epsilon},$$

and we conclude the proof invoking the assumption $F_{\sigma,\epsilon} = 0$ for any $\epsilon = D_\sigma|\text{ext}$. \blacksquare

4. A Crank-Nicolson-like pressure correction scheme

We now present a pressure correction scheme for the resolution of the low Mach number Navier-Stokes system (1). We begin by presenting the algorithm in the time semi-discrete setting (Section 4.1), then give the space discretization (Section 4.2). Using the property of the convection operator proved in Section 3, we then establish the kinetic energy identity satisfied by the scheme (Section 4.3). In this relation, a remainder term appears when the density is not constant, the time order of which is discussed (Section 4.4).

4.1. The time-marching algorithm

We consider an uniform subdivision of the interval $(0, T)$ denoted by $0 = t^0 < t^1 < \dots < t^N = T$. Let δt be the constant time step, namely $\delta t = t^{n+1} - t^n$ for any integer n in $\{0, \dots, N-1\}$. Let n in $\{0, \dots, N-1\}$ be fixed and let p^n , θ^n and ρ^{n-1} , ρ^n , \mathbf{u}^n be given such that

$$\frac{\rho^n - \rho^{n-1}}{\delta t} + \text{div}(\rho^n \mathbf{u}^n) = 0.$$

The Crank-Nicolson-like time splitting algorithm consists in four steps performed successively:

- 1- **Balance equation for θ** – Solve for θ^{n+1} :

$$\left| \begin{array}{l} \frac{1}{\delta t} (\rho^n \theta^{n+1} - \rho^{n-1} \theta^n) + \text{div}(\rho^n \theta^{n+1} \mathbf{u}^n) - \text{div}(\lambda \nabla \theta^{n+1}) = 0 \quad \text{in } \Omega, \\ \nabla \theta^{n+1} \cdot \mathbf{n} = 0 \quad \text{on } \partial\Omega. \end{array} \right.$$

- 2- **Update of the density** – Update the density with the equation of state:

$$\rho^{n+1} = \varrho(\theta^{n+1}).$$

this is easily done here, since this matrix is diagonal (which is consistent with a finite volume discretization of the convection operator, as studied in Section 3). Once the pressure increment is known, we deduce the values of the pressure and the end-of-step velocity.

The time accuracy of this algorithm is analyzed, for a model problem (namely the time-dependent incompressible Stokes problem) in [6].

Remark 3 (Splitting error in time) This algorithm is formally first order in time when the density varies with time, thus, even if we have derived the prediction and correction steps by using a Crank-Nicolson like technique, we cannot expect a second order convergence in this case. Our aim here is only to limitate the dissipation defect of the scheme.

Remark 4 (Convection operator for θ) At the continuous level, θ satisfies a maximum principle. The essential argument which yields this conclusion is that the convection operator in the conservation equation for θ may be recast, using the mass balance equation, as a transport operator:

$$\partial_t(\rho\theta) + \operatorname{div}(\rho\theta\mathbf{u}) = \rho (\partial_t(\theta) + \nabla(\theta) \cdot \mathbf{u}).$$

To obtain this property at the discrete level, we thus have to build a convection operator consistent with the mass balance [19] (in other words, which vanishes because of the mass balance equation for constant θ fields). To this purpose, once again, we have to shift in time the density fields in the time derivative term. Note however that, at the fully discrete level, we fall short to obtain a discrete maximum principle in the general case, since the Laplace operator we use enjoys this property only for specific meshes (see Remark 5 below).

4.2. Fully discrete scheme

Using the construction of the velocity convection operator presented in Subsection 3.2 in the discrete momentum and mass balance equations, the fully discrete form of the numerical algorithm proposed above consists in the following steps.

We assume that $(\rho_K^{n-1})_{K \in \mathcal{M}}$, $(\rho_K^n)_{K \in \mathcal{M}}$, $(\theta_K^n)_{K \in \mathcal{M}}$, $(\mathbf{u}_\sigma^n)_{\sigma \in \mathcal{E}}$ and $(p_K^n)_{K \in \mathcal{M}}$ are known, and we suppose that:

$$\frac{|K|}{\delta t}(\rho_K^n - \rho_K^{n-1}) + \sum_{\sigma \in \mathcal{E}(K)} F_{K,\sigma}^n = 0,$$

where, for $\sigma \in \mathcal{E}_{\text{ext}}$, $\sigma = K|\text{ext}$, $F_{K,\sigma}^n = 0$ and for $\sigma \in \mathcal{E}_{\text{int}}$, $\sigma = K|L$, the mass flux $F_{K,\sigma}^n$ is a given function of ρ_K^n , ρ_L^n and \mathbf{u}_σ^n (see the discretization of the mass balance equation in Step 4 below).

Then we perform successively:

- 1– **Balance equation for θ** – Solve for $(\theta_K^{n+1})_{K \in \mathcal{M}}$:

$$\forall K \in \mathcal{M}, \quad \frac{|K|}{\delta t}(\rho_K^n \theta_K^{n+1} - \rho_K^{n-1} \theta_K^n) + \sum_{\sigma \in \mathcal{E}(K)} F_{K,\sigma}^n \theta_\sigma^{n+1} + \lambda \Delta_K(\theta^{n+1}) = 0,$$

where θ_σ is an upwind approximation for the unknown θ at the face σ and Δ_K is a finite volume approximation of the Laplace operator: for admissible meshes (*i.e.* here, for structured grids), we use the usual two-point flux approximation, while the variant

of the SUSHI method using only cell centered unknowns [9, 28] is implemented when the mesh is unstructured.

- 2– **Update of the density** – Compute the end-of-step density with the equation of state:

$$\forall K \in \mathcal{M}, \quad \rho_K^{n+1} = \varrho(\theta_K^{n+1}).$$

- 3– **Velocity prediction** – Disregarding for a while the boundary conditions, this step consists in solving for the predicted velocity unknowns $(\tilde{\mathbf{u}}_\sigma^{n+1})_{\sigma \in \mathcal{E}}$, the following system:

$$\begin{aligned} \forall \sigma \in \mathcal{E}, \text{ for } 1 \leq i \leq d, \\ \mathbf{e}^{(i)} \cdot \left[\frac{|D_\sigma|}{\delta t} (\rho_\sigma^n \tilde{\mathbf{u}}_\sigma^{n+1} - \rho_\sigma^{n-1} \mathbf{u}_\sigma^n) + \sum_{\varepsilon \in \tilde{\mathcal{E}}(D_\sigma)} F_{\sigma,\varepsilon}^n \tilde{\mathbf{u}}_\varepsilon^{n+1/2} + |D_\sigma| (\nabla p^n)_\sigma \right] \\ + \sum_{K \in \mathcal{M}} \int_K \tau(\tilde{\mathbf{u}}^{n+1/2}) : \nabla \varphi_\sigma^{(i)} \, d\mathbf{x} = 0, \quad (21) \end{aligned}$$

where we recall that $\tilde{\mathbf{u}}^{n+1/2} = (\tilde{\mathbf{u}}^{n+1} + \mathbf{u}^n)/2$. The convection operator (*i.e.* the computation of the edges density ρ_σ , of the mass fluxes at the dual faces $(F_{\sigma,\varepsilon})$ and the (centered) approximation $\tilde{\mathbf{u}}_\varepsilon^{n+1/2}$ of the velocity at the dual faces) is described in Section 3.1. The pressure gradient term reads:

$$|D_\sigma| (\nabla p^n)_\sigma \cdot \mathbf{e}^{(i)} = - \sum_{K \in \mathcal{M}} \int_K p^n \operatorname{div} \varphi_\sigma^{(i)} \, d\mathbf{x},$$

and so, for any internal edge:

$$\forall \sigma \in \mathcal{E}_{\text{int}}, \quad \sigma = K|L, \quad |D_\sigma| (\nabla p^n)_\sigma = |\sigma| (p_L^n - p_K^n) \mathbf{n}_{K,\sigma}.$$

On an external face, the impermeability boundary condition must be taken into account by (possibly, *i.e.* if the normal of the face is not colinear to a coordinate axis) making a change of unknowns for the velocity to make appear the component(s) of the velocity tangent and normal to the boundary, and this latter is prescribed to zero; at each $\sigma \in \mathcal{E}_{\text{ext}}$, an equation is thus suppressed from the system. Since the pressure gradient at a face σ is normal to σ , it is thus useless to define it for $\sigma \in \mathcal{E}_{\text{ext}}$. Note that, since the Neumann boundary associated to the tangential component(s) is homogeneous, no extra surface term appears from the integration by part of the viscous term.

- 4– **Velocity and pressure correction step** – Find the end-of-step velocity unknowns $(\mathbf{u}_\sigma^{n+1})_{\sigma \in \mathcal{E}}$ and the pressure unknowns $(p_K^{n+1})_{K \in \mathcal{M}}$ such that

$$\left| \begin{aligned} \forall \sigma \in \mathcal{E}_{\text{int}}, \quad & \frac{|D_\sigma|}{\delta t} \rho_\sigma^n (\mathbf{u}_\sigma^{n+1} - \tilde{\mathbf{u}}_\sigma^{n+1}) + \frac{1}{2} |D_\sigma| (\nabla (p^{n+1} - p^n))_\sigma = 0, \\ \forall K \in \mathcal{M}, \quad & \frac{|K|}{\delta t} (\rho_K^{n+1} - \rho_K^n) + \sum_{\sigma \in \mathcal{E}(K)} F_{K,\sigma}^{n+1} = 0. \end{aligned} \right. \quad (22)$$

Note that, since the pressure gradient is normal to a face and the velocity normal to the boundary is prescribed to zero, the velocity on the boundary is left unchanged, at this

step. This explains why the system associated to the velocity correction (first equation of (22)) may be restricted to internal faces.

Since the density is given by the equation of state, there is no need to use upwinding in the mass balance equation (by opposition with compressible flows problem [16], for instance, where upwinding ensures the positivity of ρ), and we thus use a centered approach:

$$\begin{aligned} \forall \sigma \in \mathcal{E}_{\text{int}}, \sigma = K|L, & \quad F_{K,\sigma}^{n+1} = |\sigma| \frac{(\rho_K^{n+1} + \rho_L^{n+1})}{2} \mathbf{u}_\sigma^{n+1} \cdot \mathbf{n}_{K,\sigma}, \\ \forall \sigma \in \mathcal{E}_{\text{ext}}, \sigma = K|\text{ext}, & \quad F_{K,\sigma}^{n+1} = 0. \end{aligned}$$

Remark 5 (Maximum principle for θ and positivity of the density) For structured meshes, the upwind choice for θ in the discrete convection operator of the associated balance conservation equation, together with the particular form of the Laplace operator, ensures a discrete maximum principle, and thus the positivity of the density. When the mesh is unstructured, no such property is known for the SUSHI scheme. However, we did not observe under- or overshoots in practical computations.

4.3. Kinetic energy identity

We first define the following discrete semi-norm for the pressure p in M_h :

$$|p|_{1,\mathcal{M},\rho}^2 = \sum_{\sigma \in \mathcal{E}_{\text{int}}} \frac{1}{\rho_\sigma |D_\sigma|} |(\nabla p)_\sigma|^2 = \sum_{\substack{\sigma \in \mathcal{E}_{\text{int}}, \\ \sigma = K|L}} \frac{|\sigma|^2}{\rho_\sigma |D_\sigma|} (p_K - p_L)^2. \quad (23)$$

This norm is well defined if the density is positive, which is always the case in practice (see Remark 5).

The application of the discrete counterpart of the continuous procedure described in introduction yields to the following result.

Proposition 4.1 (Global kinetic energy balance) *Let us assume that $F_{\sigma,\varepsilon} = 0$ for any $\varepsilon = D_\sigma|\text{ext}$. Provided that the discrete mass balance (9) holds, we have, $\forall n \in \{0, \dots, N-1\}$:*

$$\begin{aligned} \frac{1}{2} \sum_{\sigma \in \mathcal{E}} |D_\sigma| (\rho_\sigma^n |\mathbf{u}_\sigma^{n+1}|^2 - \rho_\sigma^{n-1} |\mathbf{u}_\sigma^n|^2) + \delta t \sum_{K \in \mathcal{M}} \int_K \tau(\tilde{\mathbf{u}}^{n+1/2}) : \nabla(\tilde{\mathbf{u}}^{n+1/2}) \, dx \\ - \frac{\delta t}{2} \sum_{K \in \mathcal{M}} \sum_{\sigma \in \mathcal{E}(K)} |\sigma| (p_K^{n+1} \mathbf{u}_\sigma^{n+1} + p_K^n \mathbf{u}_\sigma^n) \cdot \mathbf{n}_{K,\sigma} + \mathcal{D}^{n+1} = 0, \end{aligned}$$

where \mathcal{D}^{n+1} stands for a numerical remainder term which reads:

$$\mathcal{D}^{n+1} = \frac{\delta t^2}{8} (|p^{n+1}|_{1,\mathcal{M},\rho^n}^2 - |p^n|_{1,\mathcal{M},\rho^n}^2) - \frac{1}{8} \sum_{\sigma \in \mathcal{E}} |D_\sigma| (\rho_\sigma^n - \rho_\sigma^{n-1}) |\tilde{\mathbf{u}}_\sigma^{n+1} - \mathbf{u}_\sigma^n|^2. \quad (24)$$

Proof. Let $0 \leq n \leq N-1$ and $\sigma \in \mathcal{E}$. Let us multiply the discrete velocity prediction step (21) associated to the face σ and the component i by $(\tilde{\mathbf{u}}_\sigma^{n+1/2})_i$ for $1 \leq i \leq d$ and then sum over i .

Invoking Proposition 3.1, we get:

$$\begin{aligned} \frac{|D_\sigma|}{2\delta t} (\rho_\sigma^n |\tilde{\mathbf{u}}_\sigma^{n+1}|^2 - \rho_\sigma^{n-1} |\mathbf{u}_\sigma^n|^2) + \frac{1}{2} \sum_{\varepsilon=D_\sigma|D_{\sigma'}} F_{\sigma,\varepsilon}^n \tilde{\mathbf{u}}_\sigma^{n+1/2} \cdot \tilde{\mathbf{u}}_{\sigma'}^{n+1/2} \\ + |D_\sigma| (\nabla p^n)_\sigma \cdot \tilde{\mathbf{u}}_\sigma^{n+1/2} + |D_\sigma| (-\Delta \tilde{\mathbf{u}}^{n+1/2}) \cdot \tilde{\mathbf{u}}_\sigma^{n+1/2} + \mathcal{R}_\sigma^{n+1} = 0, \end{aligned} \quad (25)$$

where the discrete approximation of the Laplace operator applied to $\tilde{\mathbf{u}}^{n+1/2}$ reads:

$$\text{for } 1 \leq i \leq d, \quad |D_\sigma| (-\Delta \tilde{\mathbf{u}}^{n+1/2})_i = \sum_{K \in \mathcal{M}} \int_K \tau(\tilde{\mathbf{u}}^{n+1/2}) : \nabla \varphi_\sigma^{(i)} \, dx,$$

and the remainder term \mathcal{R}_σ^{n+1} reads:

$$\mathcal{R}_\sigma^{n+1} = -\frac{|D_\sigma|}{8\delta t} (\rho_\sigma^n - \rho_\sigma^{n-1}) |\tilde{\mathbf{u}}_\sigma^{n+1} - \mathbf{u}_\sigma^n|^2.$$

We now recast the first Equation of the correction step (22) as:

$$\left[\frac{|D_\sigma| \rho_\sigma^n}{2\delta t} \right]^{1/2} \mathbf{u}_\sigma^{n+1} + \left[\frac{|D_\sigma| \delta t}{8\rho_\sigma^n} \right]^{1/2} (\nabla p^{n+1})_\sigma = \left[\frac{|D_\sigma| \rho_\sigma^n}{2\delta t} \right]^{1/2} \tilde{\mathbf{u}}_\sigma^{n+1} + \left[\frac{|D_\sigma| \delta t}{8\rho_\sigma^n} \right]^{1/2} (\nabla p^n)_\sigma.$$

Taking the square of the norm of both sides of this relation, we get:

$$\begin{aligned} \frac{|D_\sigma|}{2\delta t} \rho_\sigma^n |\mathbf{u}_\sigma^{n+1}|^2 + \frac{1}{2} |D_\sigma| (\nabla p^{n+1})_\sigma \cdot \mathbf{u}_\sigma^{n+1} + \frac{\delta t}{8} \frac{|D_\sigma|}{\rho_\sigma^n} |(\nabla p^{n+1})_\sigma|^2 \\ = \frac{|D_\sigma|}{2\delta t} \rho_\sigma^n |\tilde{\mathbf{u}}_\sigma^{n+1}|^2 + \frac{1}{2} |D_\sigma| (\nabla p^n)_\sigma \cdot \tilde{\mathbf{u}}_\sigma^{n+1} + \frac{\delta t}{8} \frac{|D_\sigma|}{\rho_\sigma^n} |(\nabla p^n)_\sigma|^2. \end{aligned}$$

Summing with (25) and multiplying by δt , we obtain:

$$\begin{aligned} \frac{|D_\sigma|}{2} (\rho_\sigma^n |\mathbf{u}_\sigma^{n+1}|^2 - \rho_\sigma^{n-1} |\mathbf{u}_\sigma^n|^2) + \frac{\delta t}{2} \sum_{\varepsilon=D_\sigma|D_{\sigma'}} F_{\sigma,\varepsilon}^n \tilde{\mathbf{u}}_\sigma^{n+1/2} \cdot \tilde{\mathbf{u}}_{\sigma'}^{n+1/2} \\ + \frac{\delta t |D_\sigma|}{2} \left[(\nabla p^n)_\sigma \cdot \mathbf{u}_\sigma^n + (\nabla p^{n+1})_\sigma \cdot \mathbf{u}_\sigma^{n+1} \right] + |D_\sigma| \delta t (-\Delta \tilde{\mathbf{u}}^{n+1/2}) \cdot \tilde{\mathbf{u}}_\sigma^{n+1/2} + \mathcal{D}_\sigma^{n+1} = 0, \end{aligned} \quad (26)$$

with:

$$\mathcal{D}_\sigma^{n+1} = -\frac{|D_\sigma|}{8} (\rho_\sigma^n - \rho_\sigma^{n-1}) |\tilde{\mathbf{u}}_\sigma^{n+1} - \mathbf{u}_\sigma^n|^2 + \frac{\delta t^2}{8} \left(\frac{|D_\sigma|}{\rho_\sigma^n} |(\nabla p^{n+1})_\sigma|^2 - \frac{|D_\sigma|}{\rho_\sigma^n} |(\nabla p^n)_\sigma|^2 \right).$$

We then sum over the edges. The kinetic energy convection fluxes (*i.e.* the second term at the left-hand side) vanish by conservativity (for $\varepsilon = D_\sigma|D_{\sigma'}$, $F_{\sigma,\varepsilon}^n = -F_{\sigma',\varepsilon}^n$) and by the boundary conditions (for $\varepsilon = D_\sigma|\text{ext}$, $F_{\sigma,\varepsilon}^n = 0$). We make a discrete integration by parts in the gradient terms, *i.e.* we use the fact that, thanks to the definition of the pressure gradient and, once again, to the boundary conditions, for any discrete functions \mathbf{u} and p :

$$\sum_{\substack{\sigma \in \mathcal{E}_{\text{int}}, \\ \sigma = K|L}} |D_\sigma| (\nabla p)_\sigma \cdot \mathbf{u}_\sigma = \sum_{\substack{\sigma \in \mathcal{E}_{\text{int}}, \\ \sigma = K|L}} |\sigma| (p_L - p_K) \mathbf{n}_{K,\sigma} \cdot \mathbf{u}_\sigma = - \sum_{K \in \mathcal{M}} p_K \sum_{\sigma \in \mathcal{E}(K)} |\sigma| \mathbf{u}_\sigma \cdot \mathbf{n}_{K,\sigma}.$$

Finally, we easily get that, by definition:

$$\sum_{\sigma \in \mathcal{E}} |D_\sigma| (-\Delta \tilde{\mathbf{u}}^{n+1/2}) \cdot \tilde{\mathbf{u}}^{n+1/2} = \sum_{K \in \mathcal{M}} \int_K \tau(\tilde{\mathbf{u}}^{n+1/2}) : \nabla \tilde{\mathbf{u}}^{n+1/2} \, d\mathbf{x},$$

which concludes the proof. ■

Remark 6 (Local kinetic energy identity) Note that Equation (26) is the discrete analogue of the (local) kinetic energy identity (6), to which it may be identified term by term. Both the kinetic energy flux (second term) and the pressure gradient term (third one) are consistent with centered in time and space discretizations.

Such a relation may be used for different purposes. For instance, one may find in [16] a way to exploit such an identity to switch in Euler equations from the total energy to the internal energy balance without loosing the consistency of the scheme.

4.4. Order in time of the dissipation defect

In the previous subsection, it has been shown (Proposition 4.1) that we are able to write a discrete equation governing the variation of kinetic energy for the Crank-Nicolson-like pressure correction scheme presented before. By adding up the relation established in Proposition 4.1 for n ranging from 0 to $N - 1$, we get:

$$\begin{aligned} \frac{1}{2} \sum_{\sigma \in \mathcal{E}} |D_\sigma| (\rho_\sigma^{N-1} |\mathbf{u}_\sigma^N|^2 - \rho_\sigma^{-1} |\mathbf{u}_\sigma^0|^2) + \delta t \sum_{n=0}^{N-1} \sum_{K \in \mathcal{M}} \int_K \tau(\tilde{\mathbf{u}}^{n+1/2}) : \nabla \tilde{\mathbf{u}}^{n+1/2} \, d\mathbf{x} \\ - \frac{\delta t}{2} \sum_{n=0}^{N-1} \sum_{K \in \mathcal{M}} \sum_{\sigma \in \mathcal{E}(K)} |\sigma| (p_K^n \mathbf{u}_\sigma^n + p_K^{n+1} \mathbf{u}_\sigma^{n+1}) \cdot \mathbf{n}_{K,\sigma} + \mathcal{D} = 0, \quad (27) \end{aligned}$$

with:

$$\mathcal{D} = \frac{\delta t^2}{8} \sum_{n=0}^{N-1} \left(|p^{n+1}|_{1,\mathcal{M},\rho^n}^2 - |p^n|_{1,\mathcal{M},\rho^n}^2 \right) - \frac{1}{8} \sum_{n=0}^{N-1} \sum_{\sigma \in \mathcal{E}} |D_\sigma| (\rho_\sigma^n - \rho_\sigma^{n-1}) |\tilde{\mathbf{u}}_\sigma^{n+1} - \mathbf{u}_\sigma^n|^2.$$

Relation (27) does not provide a stability estimate, for three reasons:

- 1 - The third term at the left-hand side is the discrete counterpart of the continuous term $\int_0^T \int_\Omega p \operatorname{div} \mathbf{u} \, d\mathbf{x} \, dt$, the control of which is not possible in the low Mach number model; for an incompressible flow, this term would simply vanish.
- 2 - The first term in the remainder \mathcal{D} is not non-negative, because of the presence of different density weights in pressure semi-norms; this problem would be cured if the quantity $|p^n|_{1,\mathcal{M},\rho^n}$ were replaced by $|p^n|_{1,\mathcal{M},\rho^{n-1}}$, and this can be done by adding to the algorithm a pressure renormalization step, following the study presented in [13]. This step is not implemented here, because it does not seem to be crucial for the robustness of our scheme.
- 3 - The last term in \mathcal{D} can take any sign.

Note that none of these issues occurs when the density is constant ($\operatorname{div} \mathbf{u} = 0$ and $\mathcal{D} = 0$), so that the scheme is unconditionally stable in this case.

The quantity \mathcal{D} is a numerical remainder term, which is referred to in the sequel as the *dissipation defect* of the scheme. We now show that \mathcal{D} is formally second order in time. Indeed, we have, using Equation (23) and reordering the sum in time:

$$\begin{aligned} \frac{\delta t^2}{8} \sum_{n=0}^{N-1} \left(|p^{n+1}|_{1,\mathcal{M},\rho^n}^2 - |p^n|_{1,\mathcal{M},\rho^n}^2 \right) &= \frac{\delta t^2}{8} \left(|p^N|_{1,\mathcal{M},\rho^{N-1}}^2 - |p^0|_{1,\mathcal{M},\rho^0}^2 \right) \\ &+ \frac{\delta t^2}{8} \sum_{n=1}^{N-1} \sum_{\sigma \in \mathcal{E}_{\text{int}}} |D_\sigma| |(\nabla p^n)_\sigma|^2 \left(\frac{1}{\rho_\sigma^{n-1}} - \frac{1}{\rho_\sigma^n} \right). \end{aligned}$$

So each sum in \mathcal{D} is a product of δt^2 multiplied by a sum that behaves like $\mathcal{O}(1)$ in time.

Remark 7 (First order backward Euler time discretization) When approximating the velocity time derivative with first order backward Euler scheme [1], a similar analysis yields, for $0 \leq n \leq N-1$:

$$\begin{aligned} \frac{1}{2} \sum_{\sigma \in \mathcal{E}} |D_\sigma| (\rho_\sigma^n |\mathbf{u}_\sigma^{n+1}|^2 - \rho_\sigma^{n-1} |\mathbf{u}_\sigma^n|^2) + \delta t \sum_{K \in \mathcal{M}} \int_K \tau(\tilde{\mathbf{u}}^{n+1}) : \nabla \tilde{\mathbf{u}}^{n+1} \, d\mathbf{x} \\ - \delta t \sum_{K \in \mathcal{M}} p_K^{n+1} \sum_{\sigma \in \mathcal{E}(K)} |\sigma| \mathbf{u}_\sigma^{n+1} \cdot \mathbf{n}_{K,\sigma} + \mathcal{D}_{Euler}^{n+1} = 0, \quad (28) \end{aligned}$$

where the numerical remainder term $\mathcal{D}_{Euler}^{n+1}$ now reads:

$$\mathcal{D}_{Euler}^{n+1} = \frac{\delta t^2}{2} (|p^{n+1}|_{1,\mathcal{M},\rho^n}^2 - |p^n|_{1,\mathcal{M},\rho^n}^2) + \frac{1}{2} \sum_{\sigma \in \mathcal{E}} |D_\sigma| \rho_\sigma^n |\tilde{\mathbf{u}}_\sigma^{n+1} - \mathbf{u}_\sigma^n|^2. \quad (29)$$

Summing up Equalities (28) for n ranging from 0 to $N-1$, we get the following expression for the dissipation defect of the scheme:

$$\mathcal{D}_{Euler} = \frac{\delta t^2}{2} \sum_{n=0}^{N-1} \left(|p^{n+1}|_{1,\mathcal{M},\rho^n}^2 - |p^n|_{1,\mathcal{M},\rho^n}^2 \right) + \frac{1}{2} \sum_{n=0}^{N-1} \sum_{\sigma \in \mathcal{E}} |D_\sigma| \rho_\sigma^n |\tilde{\mathbf{u}}_\sigma^{n+1} - \mathbf{u}_\sigma^n|^2,$$

and, if, as in the Crank-Nicolson-like pressure correction scheme, the first sum behaves like $\mathcal{O}(\delta t^2)$, the second one behaves as $\mathcal{O}(\delta t)$ and the defect dissipation is thus first order in time.

5. Numerical experiments

In this section, we describe some numerical experiments performed to assess the behaviour of the Crank-Nicolson-like pressure correction scheme proposed in Section 4. To this purpose, we compare it to a classical pressure correction scheme [1], based on the same space discretization and on the first order backward Euler in time. The simulations are performed with the ISIS software [17] based on the development platform and software component library PELICANS [27], both developed at IRSN (Institut de Radioprotection et de Sûreté Nucléaire).

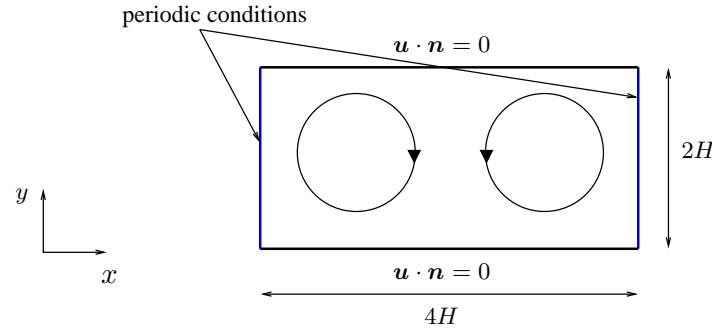


Figure 3. Vorticity decrease test case – Configuration of the test case.

5.1. Vorticity decrease in a 2D laminar channel flow

For this test case, we propose to study the decreasing rate of vortices in a 2D channel. The computational domain Ω is $(-2H, 2H) \times (-H, H)$, with $H = 1$. The flow is supposed to be periodic in the x -direction and perfect slip boundary conditions are prescribed at the lower and upper sides of the domain, as shown on Figure 3. It is initialized by two contrarotative vortices. The expression of the velocity for one vortex centered at $(0, 0)$ is:

$$\begin{aligned} u &= y \sin(\pi r)/r \\ v &= -x \sin(\pi r)/r \end{aligned}$$

with $r = \sqrt{x^2 + y^2}$ and the velocity is zero outside the vortex (for $r > 1$). By translation of this last formula, we get the expression of two vortices centered respectively at $(-1, 0)$ and $(1, 0)$ with an opposite sign. The initial velocity is defined as the sum of both vortices.

Both cases are studied here with constant and with variable densities.

The mesh is a regular grid composed of 500×250 cells. Even if there is no pressure initial condition in the Navier-Stokes system, an initial value for the pressure needs to be given to the algorithm (even if its value is not crucial for the computation, since the seminal non-incremental projection scheme [4, 33] is known to converge with a first order rate with time). We choose here to set $p^0 = 0$.

5.1.1. Constant density test case We begin the study with a simulation for a constant density (*i.e.* incompressible) flow, with $\rho = 1 \text{ kg.m}^{-3}$. The viscosity is set to $\mu = 10^{-4} \text{ Pa.s}$, so, taking $\mathbf{u}_{\max} = 1 \text{ m/s}$ for reference value for the velocity, we get for the Reynolds number:

$$Re = \frac{\rho \mathbf{u}_b H}{\mu} = 10^4.$$

Kinetic energy – The vortices slowly damp in time. Consequently, the kinetic energy decreases too (see Figure 4). Graphs showing the kinetic energy evolution for the various considered time discretizations are gathered below for time steps $\delta t = 0.1$ and $\delta t = 0.005$ (Figure 4); in addition, the results of the simulation carried out with a small time step $\delta t = 10^{-3}$ are given as a reference computation.

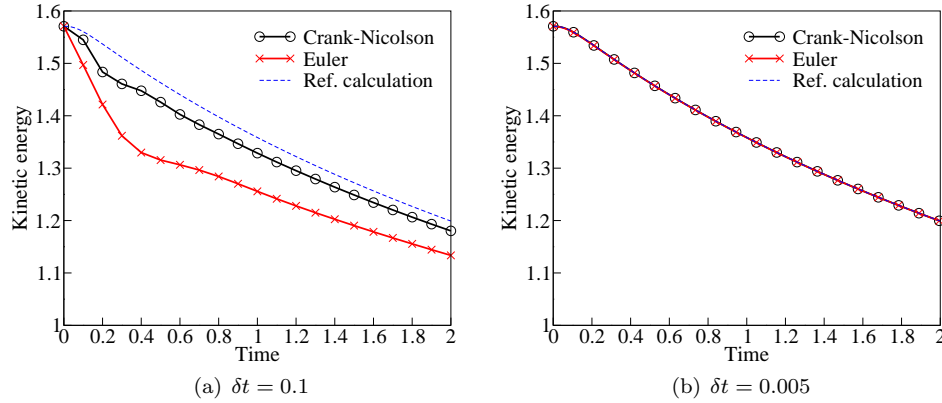


Figure 4. Vorticity decrease test case, with a constant density – Kinetic energy for Crank-Nicolson and Euler time discretizations.

For large time steps, Euler scheme dissipates more than Crank-Nicolson scheme as the kinetic energy decreases faster. For $\delta t = 0.005$ both schemes give similar results and are converged in time.

Dissipation defect – The goal of this paragraph is to illustrate the fact that the proposed time marching algorithm provides a lower dissipation defect than Euler scheme. In the definition of dissipation defect given by (24) for Crank-Nicolson and (29) for Euler, we distinguish the pressure gradient part, noted \mathcal{D}_P^n , from the kinetic energy part, noted \mathcal{D}_E^n . We draw on Figure 5 the maximum values in time \mathcal{D}_P and \mathcal{D}_E of each part as functions of the time step for both algorithms, where \mathcal{D}_P and \mathcal{D}_E are defined by ($N_0 = 0$ for the constant density case):

$$\begin{aligned}\mathcal{D}_P &= \max_{N_0 \leq n \leq N-1} \left| \sum_{k=N_0}^n \mathcal{D}_P^{k+1} \right|, \\ \mathcal{D}_E &= \max_{N_0 \leq n \leq N-1} \left| \sum_{k=N_0}^n \mathcal{D}_E^{k+1} \right|.\end{aligned}\tag{30}$$

Since the density is constant, the kinetic energy part for Crank-Nicolson scheme is zero. As expected by analysis given in Section 4.4, the pressure gradient part of the dissipation defect is of order two for both schemes and the kinetic energy part for Euler scheme is of order one.

5.1.2. Variable density test case We now turn to a variable density case. For this case, we consider θ as a mass fraction and use, for the equation of state, a mixture law standard in diphasic flows modelling:

$$\rho = \frac{1}{\frac{\theta}{\rho_1} + \frac{1-\theta}{\rho_2}},$$

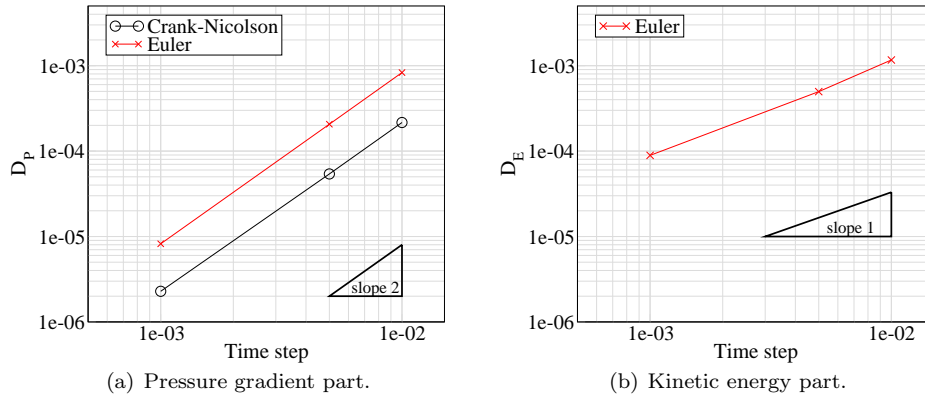


Figure 5. Vorticity decrease test case, with a constant density – Size of the dissipation defect parts as functions of time step for Crank-Nicolson and Euler time discretizations.

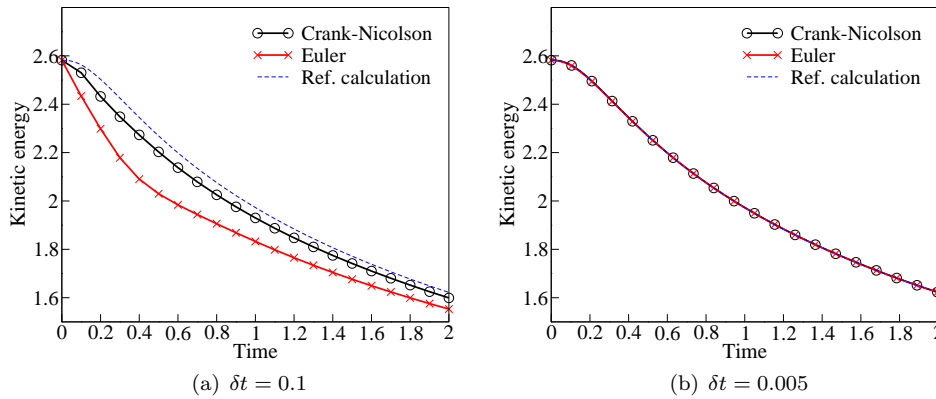


Figure 6. Vorticity decrease test case, with a variable density – Kinetic energy for Crank-Nicolson and Euler time discretizations.

where $\rho_1 = 1$ and $\rho_2 = 5$ stand for the phase densities. The initial value for θ in each vortex is:

$$\theta = \frac{1 + \cos(\pi r)}{2}.$$

Kinetic energy – The time evolution of the kinetic energy on the time interval $(0, 2)$ is represented on Figure 6, for two time steps and a reference solution obtained with $\delta t = 10^{-3}$. For large time step, it seems that the Crank-Nicolson-like scheme is still less dissipative than the Euler one. For the smallest time step $\delta t = 0.005$, the kinetic energy evolution is very similar for both schemes.

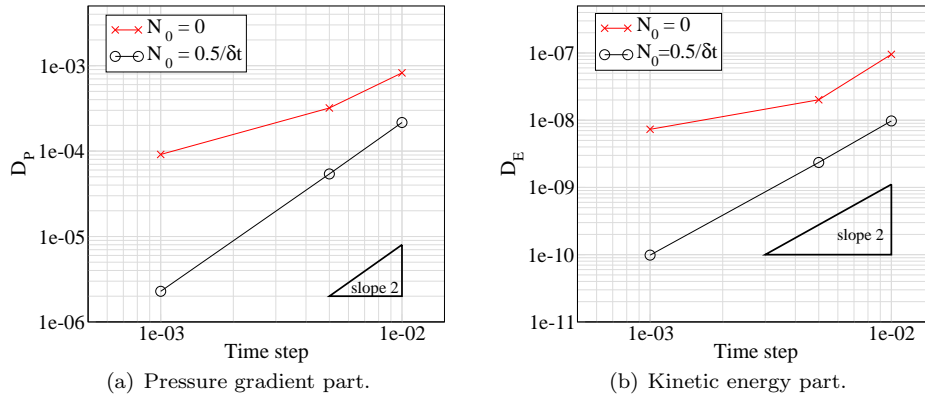


Figure 7. Vorticity decrease test case, with a variable density – Size of the dissipation defect parts for different N_0 (Equation (30)) as functions of time step for Crank-Nicolson time discretizations.

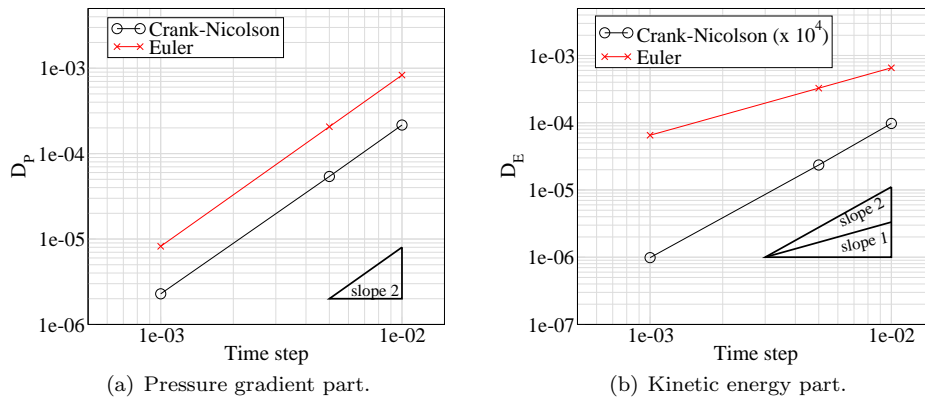


Figure 8. Vorticity decrease test case, with a variable density – Size of the dissipation defect parts as functions of time step for Crank-Nicolson and Euler time discretizations.

Dissipation defect – Here, in the definition (30), N_0 is taken large enough ($N_0 = 0.5/\delta t$) to have no impact of the initial condition. Indeed, if N_0 is chosen equal to zero, the time order of the dissipation defect parts for the Crank-Nicolson-like scheme is only one, whereas the two order is obtained for $N_0 = 0.5/\delta t$.

We plot the dissipation defect as a function of the time step on Figure 8. As in the constant density case, we observe a second-order behaviour for both schemes for the pressure gradient part of the dissipation defect. The kinetic energy part is of order one for Euler scheme and of order two for Crank-Nicolson one. It is very small using the Crank-Nicolson scheme (observe that the dissipation defect is multiplied by 10^4 in Figure 8).

5.2. 2D laminar flow around cylinder

We address in this section some test cases which are derived from a benchmark proposed in [31]. The considered case is two-dimensional, and we decompose the study in two parts: first, the flow is supposed to be homogeneous and isotherm (ρ is constant), and second the cylinder is heated. We give here a brief description of the data and refer to [31] (2D-2 case) for a complete presentation.

The geometry for both tests is sketched on Figure 9. A circle of diameter $D = 0.1\text{m}$ is included in a channel. The fluid enters the domain on the left boundary, with an imposed velocity profile:

$$u_x(0, y) = 4u_m y \frac{H - y}{H^2}, \quad u_y(0, y) = 0,$$

where $H = 0.41\text{m}$ is the height of the channel and $u_m = 1.5\text{m/s}$; a zero velocity is prescribed at the other boundaries except for the right side, where we use an outlet boundary condition.

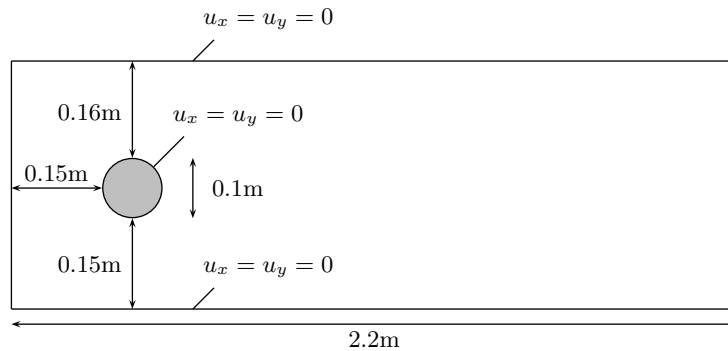


Figure 9. Geometry for the flow around a cylinder test case.

The coarse mesh (mesh#1) used for the presented computation is given on Figure 10; other meshes are refined with respect to this one, by diminishing the discretization step along some characteristic lines (the boundaries and the concentric circles around the cylinder), as reported on Table II.

Table II. Laminar flow around a cylinder – Description of the meshes used.

Computation	mesh#1	mesh#2	mesh#3	mesh#4	mesh#5
Number of cells	4033	12913	43009	76091	106101
Space unk.	12256	39014	129527	228937	409099

The flow is unsteady (see Figure 11 for a visualization at a given time), and the main characteristic flow quantities quoted in [31] are the maximum drag coefficient $c_{D_{\max}}$, the maximum lift coefficient $c_{L_{\max}}$, the Strouhal number St and an instantaneous pressure

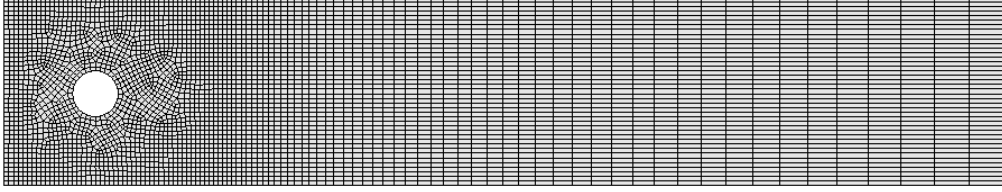
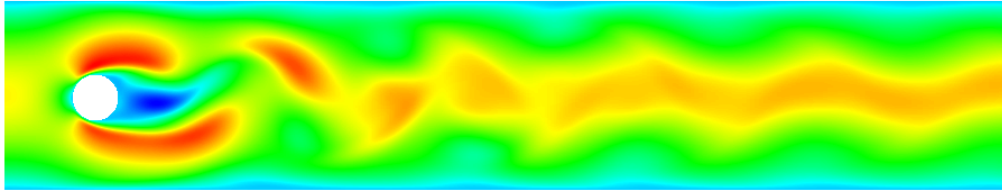


Figure 10. The coarse mesh (mesh#1).

Figure 11. Laminar flow around a cylinder – First component (x -component) of the velocity.

difference ΔP between the front and end points of the cylinder, *i.e.* the points $(0.15\text{m}, 0.20\text{m})$ and $(0.25\text{m}, 0.20\text{m})$ (see [31, section 2.2]). Drag and lift coefficients are defined as follows: denoting by S the circle and by \mathbf{u}_t the tangential component of the velocity (namely $\mathbf{u}_t = \mathbf{u} \cdot \mathbf{t}$ if \mathbf{t} designates the tangential vector to S), we first consider the corresponding forces

$$F_D = \int_S (\rho\nu \frac{\partial \mathbf{u}_t}{\partial \mathbf{n}} \mathbf{n}_y - p \mathbf{n}_x) dS, \quad F_L = - \int_S (\rho\nu \frac{\partial \mathbf{u}_t}{\partial \mathbf{n}} \mathbf{n}_x + p \mathbf{n}_y) dS.$$

Then, c_D and c_L are obtained by scaling F_D and F_L by $2/(\rho \bar{u}^2 D)$. Moreover, the Strouhal number is $St = Df/\bar{u}$, f being the frequency of separation. This frequency is assessed from temporal evolution of the lift coefficient.

Isothermal case The density is $\rho = 1\text{kg.m}^{-3}$ and the viscosity is $\mu = 0.001$ Pa.s, so the Reynolds number, defined as $Re = \rho \bar{u} D / \mu$, where $\bar{u} = 2 u_x(0, H/2) / 3 = 1$, is equal to 100.

The time step varies between 10^{-3} for the coarse mesh and $2 \cdot 10^{-4}$ for the thinnest mesh to keep a constant CFL number.

The computed values ($c_{D_{\max}}$, $c_{L_{\max}}$, St and ΔP) are gathered in Table III, as well as a plausible range for the results derived from the set of the contributions to the benchmark. Values entering this reference interval are typeset in bold.

According to Tables III and IV, both schemes give results included in the benchmark reference range, except for the Strouhal number which is underestimated by Euler scheme.

Table III. Laminar flow around a cylinder, isothermal case – Crank-Nicolson time discretization.

Computation	$c_{D\max}$	$c_{L\max}$	St	ΔP
mesh#1	3.66	0.79	0.270	2.30
mesh#2	3.41	0.95	0.294	2.45
mesh#3	3.25	0.98	0.303	2.50
mesh#4	3.23	1.00	0.303	2.49
mesh#5	3.22	1.01	0.303	2.48
Reference range [31]	3.22 – 3.24	0.99 – 1.01	0.295 – 0.305	2.46 – 2.50

Table IV. Laminar flow around a cylinder, isothermal case – Euler time discretization.

Computation	$c_{D\max}$	$c_{L\max}$	St	ΔP
mesh#1	3.62	0.75	0.269	2.36
mesh#2	3.40	0.92	0.288	2.45
mesh#3	3.25	0.97	0.294	2.49
mesh#4	3.23	0.98	0.294	2.484
mesh#5	3.22	1.00	0.294	2.478
Reference range [31]	3.22 – 3.24	0.99 – 1.01	0.295 – 0.305	2.46 – 2.50

Anisothermal case In this part, with the same configuration as in the previous part, the cylinder is heated at a temperature T_h . The fluid enters in the domain with a cold temperature T_c and the wall temperature is also fixed at T_c .

We propose to study the influence of the parameter ϵ defined by:

$$\epsilon = \frac{T_h - T_c}{T_h + T_c}.$$

The parameter varies between 0 (isothermal case) to 0.8. For this study, the Prandtl number is equal to 0.7, the viscosity is fixed to 0.001 Pa.s and the specific heat to 1000 J.kg⁻¹.K⁻¹.

Here, the scalar θ is the temperature T and the density verifies the dilatable gas law:

$$\rho = \rho_0 \frac{T_0}{T},$$

where $T_0 = T_c$ and $\rho_0 = 1 \text{ kg.m}^{-3}$. As the mesh is unstructured, the SUSHI scheme is used for the approximation of the Laplace operator (see Remark 5) and the MUSCL scheme for the convective term [28] in the balance equation for θ . The time step satisfies a CFL condition required by MUSCL scheme and varies between $2 \cdot 10^{-5}$ and 10^{-4} during the computations. The computations are performed with the thinnest mesh of the isothermal case (mesh#5).

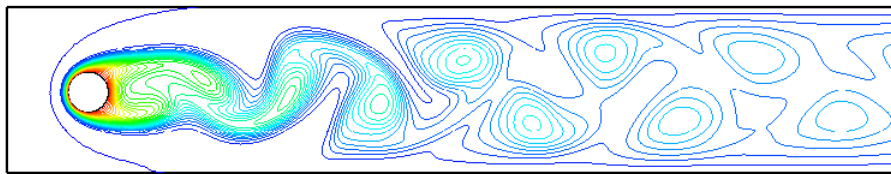
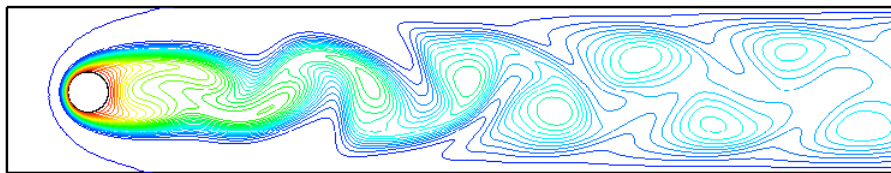
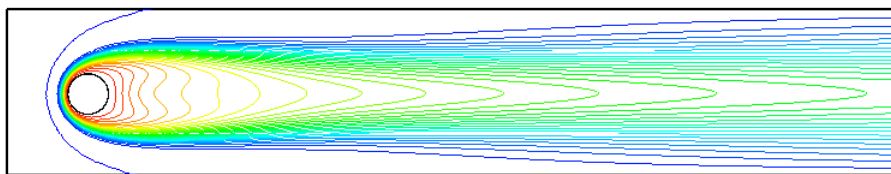
On Figure 12, the density field is represented for $\epsilon = 0.4, 0.6, 0.8$. For small values of ϵ , as for the isothermal case, the flow is unsteady and oscillations appear in the wake of the cylinder. For $\epsilon = 0.4$, the amplitudes seem to be greater than for $\epsilon = 0.6$. This behavior is coherent with an increase of Strouhal number when ϵ increases (see Table V). For $\epsilon = 0.8$, contrary to the other computations, the flow is steady and no oscillation appears.

Heating the cylinder leads to a depressurization behind the cylinder greater than for isothermal case. The pressure difference between two points of the cylinder increases with ϵ (see Table V).

The drag coefficient increases with ϵ whereas the lift coefficient decreases. For the steady case ($\epsilon = 0.8$), the lift coefficient is very small and its value is similar to the reference value given in the benchmark [31] for 2D steady case.

Table V. Laminar flow around a heated cylinder – Drag and lift coefficients, Strouhal number and ΔP for several ϵ .

Computation	$c_{D\max}$	$c_{L\max}$	St	ΔP
isotherm	3.22	1	0.303	2.48
$\epsilon = 0.4$	3.54	0.56	0.316	2.59
$\epsilon = 0.6$	3.84	0.236	0.342	2.71
$\epsilon = 0.8$	4.62	0.0055	steady	3.04

(a) $\epsilon = 0.4$ (b) $\epsilon = 0.6$ (c) $\epsilon = 0.8$ Figure 12. Laminar flow around a heated cylinder – Density field isolines for several ϵ at time $t = 10$ s.

5.3. 3D turbulent mixing layer

We consider here a three dimensional vertical turbulent channel of water $\Omega = [-0.2; 0.2] \times [-0.01; 1.20] \times [-0.2; 0.2]$ (in meters), with inlet boundary conditions imposed on the bottom plane $y = -0.01$ and outlet boundary conditions on the upper plane $y = 1.20$. Slip boundary conditions are prescribed on the lateral planes of Ω . Besides, the channel is divided at the bottom in two equal parts of different mass flows by a vertical plate spreading out from $y = -0.01$ to $y = 0$. The injection velocity $\mathbf{u}_1 = 0.54\text{m.s}^{-1}$ of the right side of the separation is greater than the left one $\mathbf{u}_2 = 0.22\text{m.s}^{-1}$, generating a turbulent mixing layer (see Figure 13). The flow is incompressible and the density and the viscosity are respectively fixed at 1000 kg.m^{-3} and 0.001 Pa.s . Experimental tests provide cutlines of the mean velocities and the root mean square (rms) velocity profiles measured at several heights (see [30]) defined as follows: let us consider a time-interval $[t; t']$ (when the fully turbulent state is reached, *i.e.* $t = 6\text{ s}$ and $t' = 20\text{ s}$ for this simulation) discretized by $t \leq \delta t_0 \leq \dots \leq \delta t_L = t'$, then for a cell K , we set

$$\begin{aligned} \langle U_y \rangle_{|K} &= \frac{1}{t' - t} \sum_{j=0}^L \frac{\delta t_j}{|K|} \int_K U_y(\mathbf{x}, t_{init} + \delta t_j) d\mathbf{x}, \\ (U_y)_{rms} &= \sqrt{\langle U_y^2 \rangle_{|K} - \langle U_y \rangle_{|K}^2}. \end{aligned}$$

The mesh is constituted of $90 \times 90 \times 270$ cells to have an uniform grid and simulations are

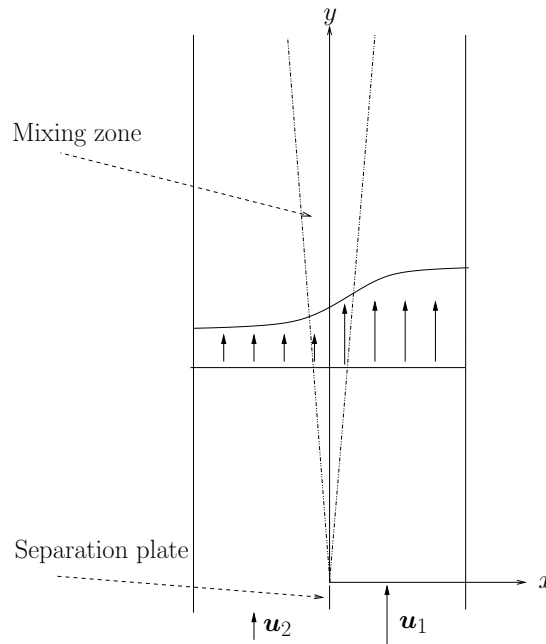


Figure 13. Turbulent mixing layer – Numerical set-up (front view).

carried out for the time steps $\delta t = 10^{-2}$ and $\delta t = 10^{-3}$ s, for time ranging from 0 to 20 s. The entering velocity field is built from experimental data with the vortex method [18] to

generate turbulence. The subgrid scale model is the Smagorinsky model ($C_s = 0.12$, [22]) and we compare the Crank-Nicolson-like pressure correction scheme introduced here to the first order backward Euler scheme.

Representations of the vorticity norm isosurfaces for the isovalue 6 are gathered on Figure 14 for several time steps.

For the time step 10^{-2} s, Figure 14 shows that vortices present more complex structures with the Crank-Nicolson-like scheme than with first backward Euler one. For $\delta t = 10^{-3}$ s, both schemes give similar results.

Comparing the outline of the time mean value of the axial velocity (denoted by $\langle U_y \rangle$) between 8 s and 20 s (see Figure 15) at $y = 0.5$, we observe that the time convergence is achieved from $\delta t = 10^{-2}$ for both schemes and a good agreement is obtained with experimental results.

Figure 16 shows the time rms axial velocity (denoted by $(U_y)_{rms}$) for time ranging from 8 s to 20 s. Contrary to the mean velocity, a difference is observed between both schemes at $\delta t = 10^{-2}$. The Crank-Nicolson-like scheme enables to compute correctly the peak which is not the case for the Euler scheme. For $\delta t = 10^{-3}$, both schemes seem to have achieved convergence in time.

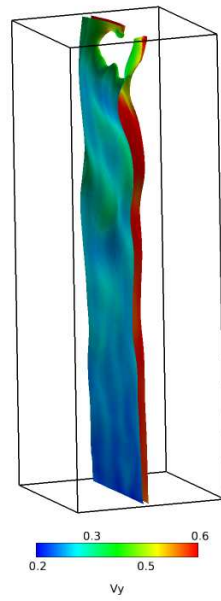
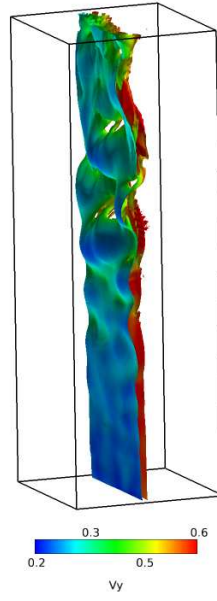
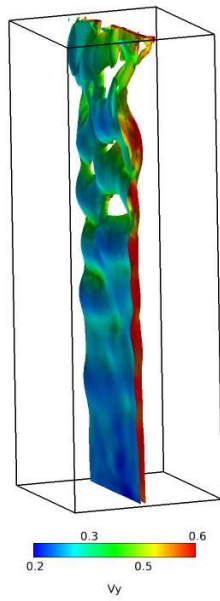
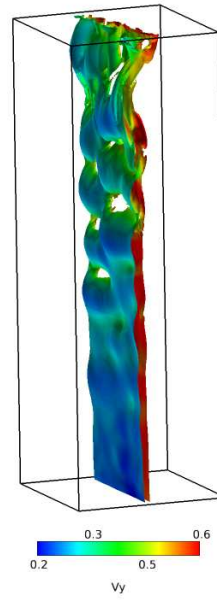
(a) Euler, $\delta t = 10^{-2}$.(b) Crank-Nicolson, $\delta t = 10^{-2}$.(c) Euler, $\delta t = 10^{-3}$.(d) Crank-Nicolson, $\delta t = 10^{-3}$.

Figure 14. Turbulent mixing layer – Vorticity norm isosurface for the isovalue 6 at time 20 s.

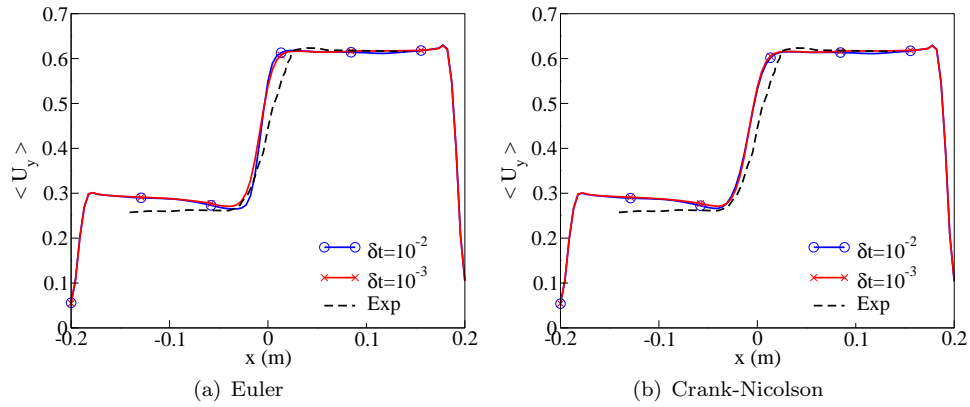


Figure 15. Turbulent mixing layer – Time averaged axial velocity at $y = 0.5$ and $z = 0$.

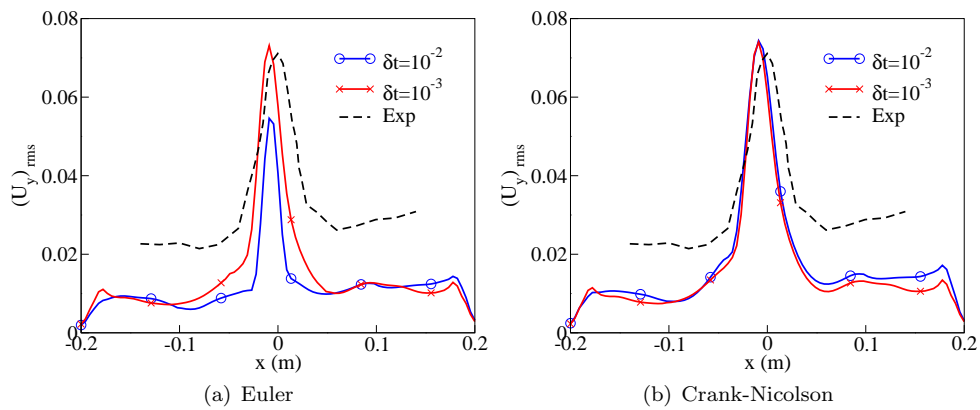


Figure 16. Turbulent mixing layer – Time rms axial velocity at $y = 0.5$ and $z = 0$.

6. Conclusion

This paper is devoted to the construction of a stable finite volume convection operator defined on a dual mesh and based on the Crank-Nicolson-like scheme in time, for a Rannacher-Turek finite element discretization on the primal mesh of the momentum equation. We prove the stability of this discretization and then use it to build a pressure correction scheme which is proved to be less dissipative than the one obtained with the usual Euler discretization in time. This work can be adapted in a straightforward way to the case of the Crouzeix-Raviart finite element discretization on triangle meshes. Furthermore, we derive a discrete kinetic energy identity and estimate the size of the dissipation defect. The scheme proposed is adapted to the Large Eddy Simulation approach because it provides a kinetic energy control and has a low dissipation defect. Therefore, we illustrate the possibilities of the scheme with various tests, incompressible or compressible, in both two and three-dimensional cases.

REFERENCES

1. G. Ansanay-Alex, F. Babik, J.-C. Latché, and D. Vola. An L2-Stable Approximation of the Navier-Stokes Convection Operator for Low-Order Non-Conforming Finite Elements. *International Journal For Numerical Methods In Fluids*, 66:555–580, 2011.
2. P. Beaudan and P. Moin. Numerical Experiments on the Flow Past a Circular Cylinder at Sub-Critical Reynolds Number. *Technical Report, TF-62, Department of Mechanic Engineering, Stanford University*, 1994.
3. F. Brezzi and M. Fortin. *Mixed and Hybrid Finite Element Methods*. Number 15 in Springer Series in Computational Mathematics. Springer-Verlag, 1991.
4. A.J. Chorin. Numerical Solution of the Navier-Stokes Equations. *Mathematics of Computation*, 22:745–762, 1968.
5. P. G. Ciarlet. Handbook of Numerical Analysis: Finite Elements Methods – Basic Error Estimates for Elliptic Problems. In P. Ciarlet and J.L. Lions, editors, *Handbook of Numerical Analysis, Volume II*. North Holland, 1991.
6. F. Dardalhon, S. Minjeaud, and J.-C. Latché. Analysis of a Projection Method for Low-Order Nonconforming Finite Elements. *IMA Journal of Numerical Analysis*, 2012.
7. O. Desjardins, G. Blanquart, G. Balarac, and H. Pitsch. High Order Conservative Finite Difference Scheme for Variable Density Low Mach Number Turbulent Flows. *Journal of Computational Physics*, 227, 2008.
8. F. Ducros, F. Laporte, T. Soulres, P. Moinat, and B. Caruelle. High-Order Fluxes for Conservative Skew-Symmetric-Like Schemes in Structured Meshes: Application to Compressible Flows. *Journal of Computational Physics*, 161(1):114–139, 2000.
9. R. Eymard, T. Gallouet, and R. Herbin. Discretization of Heterogeneous and Anisotropic Diffusion Problems on General Nonconforming Meshes SUSHI: a Scheme using Stabilisation and Hybrid Interfaces 1. *Numerical Methods for Partial Differential Equations*, 30:1009–1043, 2009.
10. F.N. Felten and T.S. Lund. Kinetic Energy Conservation Issues Associated with the Collocated Mesh Scheme for Incompressible Flow. *Journal of Computational Physics*, 215:465–484, 2006.
11. L. Gastaldo, R. Herbin, W. Kheriji, C. Lapuerta, and J.-C. Latché. Staggered Discretizations, Pressure Correction Schemes and all Speed Barotropic Schemes. *Finite Volumes for Complex Applications 6, Prague*, 2:39–55, 2011.
12. L. Georges, G. Winckelmans, and P. Geuzaine. Improving Shock-Free Compressible RANS Solvers for LES on Unstructured Meshes. *Journal of Computational Applied Mathematics*, 215:419–428, 2008.
13. J.-L. Guermond and L. Quartapelle. A Projection FEM for Variable Density Incompressible Flows. *Journal of Computational Physics*, 165:167–188, 2000.
14. By F. Ham, K. Mattsson, and G. Iaccarino. Accurate and Stable Finite Volume Operators for Unstructured Flow Solvers. *Techniques*, pages 243–261, 2006.
15. F.H. Harlow and J.E. Welch. Numerical Calculations of Time Dependent Viscous Incompressible Flow of Fluid with a Free Surface. *Physics of Fluids*, 8:2182–2189, 1965.
16. R. Herbin, W. Kheriji, and J.-C. Latché. Staggered Schemes for All Speed Flows. *ESAIM proceedings*, 35:122–150, 2012.

17. ISIS. A CFD computer code for the simulation of reactive turbulent flows.
<https://gforge.irsnn.fr/gf/project/isis>.
18. N. Jarrin, S. Benhamadouche, D. Laurence, and R. Prosser. A Synthetic-Eddy-Method for Generating Inflow Conditions for Large-Eddy Simulation. *International Journal of Heat and Fluid Flow*, 27:585–593, 2006.
19. B. Larroutou. How to Preserve the Mass Fractions Positivity when Computing Compressible Multi-Component Flows. *Journal of Computational Physics*, 95:59–84, 1991.
20. D.K. Lilly. On the Computational Stability of Numerical Solutions of Time-Dependent Non-Linear Geophysical Fluid Dynamics Problems. *Monthly Weather Review.*, 93:11–26, 1965.
21. A. Majda and J. Sethian. The Derivation and Numerical Solution of the Equations for Zero Mach Number Combustion. *Combustion Science and Techniques*, 42:185–205, 1985.
22. M. Milelli. *A Numerical Analysis of Confined Turbulent Bubble Plumes*. PhD thesis, Swiss Federal Institute of Technology, Zurich, 2002.
23. R. Mittal and P. Moin. Suitability of Upwind-Biased Finite Difference Schemes for Large-Eddy Simulation of Turbulent Flows. *AIAA Journal*, pages 1415–17, 1997.
24. Y. Morinishi. Skew-Symmetric Form of Convective Terms and Fully Conservative Finite Difference Schemes for Variable Density Low-Mach Number Flows. *Journal of Computational Physics*, 229:276–300, 2010.
25. Y. Morinishi, T. S. Lund, O. V. Vasilyev, and P. Moin. Fully Conservative Higher Order Finite Difference Schemes for Incompressible Flow. *Journal of Computational Physics*, 143:90–124, 1998.
26. F. Nicoud. Conservative High-Order Finite-Difference Schemes for Low-Mach Number Flows. *Journal of Computational Physics*, 158:71–97, 2000.
27. PELICANS. Collaborative development environment.
<https://gforge.irsnn.fr/gf/project/pelicans>.
28. L. Piar, F. Babik, R. Herbin, and J.-C. Latché. A Formally Second-Order Cell Centered Scheme for Convection-Diffusion Equations on General Grids. *International Journal for Numerical Methods in Fluids*, published online DOI: 10.1002/fld.3688.
29. R. Rannacher and S. Turek. Simple Nonconforming Quadrilateral Stokes Element. *Numerical Methods for Partial Differential Equations*, 8:97–111, 1992.
30. V. Roig. *Zone de Melange d'Écoulements Diphasiques Bulles*. PhD thesis, University of Toulouse, 1993.
31. M. Schäfer and S. Turek. Benchmark Computations of Laminar Flow Around a Cylinder. In E.H. Hirschel, editor, *Flow Simulation with High-Performance Computers II*, volume 52 of *Notes on Numerical Fluid Mechanics*, pages 547–566, 1996.
32. P. K. Subbareddy and G. V. Candler. A Fully Discrete, Kinetic Energy Consistent Finite-Volume Scheme for Compressible Flows. *Journal of Computational Physics*, 228:1347–1364, 2009.
33. R. Temam. Sur l'Approximation de la Solution des Equations de Navier-Stokes par la Méthode des Pas Fractionnaires II. *Archive for Rational Mechanics and Analysis*, 33:377–385, 1969.
34. O. Vasilyev. High Order Finite Difference Schemes on Non-Uniform Meshes with Good Conservation Properties. *Journal of Computational Physics*, 157(2):746–761, 2000.
35. R. W. C. P. Verstappen and A. E. P. Veldman. Symmetry-Preserving Discretization of Turbulent Flow. *Journal of Computational Physics*, 187:343–368, 2003.